

Cache Revive: Tuning Retention times of STT-RAM Caches for Enhanced Performance in CMPs.

Anonymous MICRO submission

Paper ID 761

Abstract

Spin-Transfer Torque RAM (STT-RAM) is a CMOS compatible emerging non-volatile memory (NVM) technology that has the potential to replace the conventional on-chip SRAM caches for designing a more efficient memory hierarchy for future multicore architectures. However, its high write latency and dynamic write energy are major obstacles for being competitive with the SRAM-based cache hierarchy. On the other hand, STT-RAM technology has another adaptable feature that it is possible to reduce its write latency by reducing its retention time, thereby making it volatile. In this paper, we exploit this volatile property of the STT-RAM for designing an efficient L2 cache architecture. The paper addresses several critical design issues such as how do we decide a suitable retention time for last level cache, what is the relationship between retention time and write latency, and how do we architect the cache hierarchy with a volatile STT-RAM. In this paper, we propose to trade off the non-volatility (data retention time) for better write performance/energy in STT-RAM cache design. We study two data-retention relaxation cases, one with data retention time of 1 second, which satisfies the lifetime requirement of typical cache blocks; and the other one with data retention time of 1ms, which is a more aggressive design for better performance/energy gains but a data refreshing mechanism is needed. In the aggressive data retention time relaxation design, for the rest of the cache blocks that have a higher inter-write time than the STT-

RAM retention time, we propose an architectural solution to identify these blocks with a per block 2 bit counter, temporarily save a limited number of MRU blocks in a buffer, and write-back the rest of the dirty blocks to avoid any data loss. Our experiments with 4 and 8-core architectures with an SRAM-based L1 cache and STT-RAM-based L2 cache indicate that not only we can eliminate the high write overhead of an NVM STT-RAM, but can provide on an average 10-12% improvement in IPC compared to the traditional SRAM-based design, while reducing the energy consumption significantly

1. Introduction

Designing an efficient memory hierarchy for multicore architectures is a critical but challenging problem. As the number of cores on a chip increases with technology scaling, the demand on the on-chip memory would increase significantly, thereby worsening the memory wall problem [?]. The memory wall problem is critical both from the performance (memory density) and power perspectives. Thus novel technology, circuit and architectural techniques are currently being explored to address the memory wall problem for many core systems.

Spin-Transfer Torque RAM (STT-RAM) is a promising memory technology that delivers on many aspects desirable of an universal memory. It has the potential to replace the conventional on-chip SRAM caches because of its higher density, competitive read times and lower leakage power consumption compared to SRAM. However, the high write latencies and write energy are key drawbacks of this technology for providing competitive or better performance compared to the SRAM-based cache hierarchy. Consequently, recent efforts have focused on masking the effects of high write latencies and write energy at the architectural level []. In contrast to these architectural approaches, a recent work explored the feasibility of relaxing STT-RAM data retention times to reduce both write latencies and write energy []. This adaptable feature of tuning the data retention time can be exploited in several dimensions. The focus of this paper is to tune this data retention time to closely match the required lifetime of the last level cache line blocks to achieve significant performance and energy gains. In this context, the paper addresses several design issues such as how to decide an appropriate retention time for the last level cache, what is

the relationship between retention time and write latency, and how do we architect the cache hierarchy with a volatile STT-RAM.

The non-volatile nature and non-destructive read ability of STT-RAM provides a key difference with regard to traditional on-chip cache design with SRAM technology. However, for many applications, it is sufficient if the data stored in the last level of a cache hierarchy remains valid for a few tens of milliseconds. Consequently, the duration of data retention in STT-RAM is an obvious candidate for device optimization for cache design. We, therefore, conduct an application-driven study to analyze the inter-write times of the L2 cache blocks to decide a suitable data retention time. Although lifetime analysis of cache lines has been conducted earlier to improve performance and reduce power consumption [], we revisit this topic with a different intention - correlating STT-RAM data retention time to cache lifetime. An extensive analysis of PARSEC and SPEC benchmarks using the M5 simulator [] indicates that the average inter-write times for most of the L2 cache blocks is around 10ms, and thus, we advocate our STT-RAM design with this retention time.

We conduct a detailed device level analysis of the STT-RAM cells to analyze the write current versus write pulse width tradeoffs, cell area analysis, and retention time stability analysis to capture the relationship between area, read/write latency and leakage power as a function of the retention time. Our observations, in contrast to the results reported in [] indicate that retention times in the range of ms are probably more achievable than in the micro second range. Thus, using this ms range retention time model, we then propose effective architectural techniques to avoid any data loss due the volatile STT-RAM-based cache hierarchy.

A key challenge in determining a suitable data retention times for the STT-RAM is to balance the reduced write latency of cells with lower retention time with the overhead for data refresh or write back of cache lines with longer lifetimes. In this paper, we compare 3 different STT-RAM based cache designs: (1) STT-RAM cache without retention time relaxation (< 10 years of data retention time); (2) STT-RAM cache with retention time of 1 second, which is long enough for the lifetime of majority of the cache lines and therefore no refreshing overhead is incurred; (3) STT-RAM cache with retention time of 10ms, which is a more aggressive design with better performance/energy gain but a data refreshing

technique is needed for correct operations since cache lines that have lifetimes exceeding 10ms are likely to loose data. Thus, we propose simple extensions to the L2 cache design for avoiding any data loss. This include a simple 2-bit counter like the victim cache [] to keep track of the lifetime of all the cache blocks and a small buffer to temporarily store the blocks whose time has exceeded the retention time. We conduct execution-driven analysis of our proposed techniques using the M5 simulator and a suite of PARSEC and SPEC benchmarks. The main contributions of this work are the following:

Detailed characterization of STT-RAM volatile property: We present a detailed device characterization of data retention tunability in STT-RAM Cells providing insight to the underlying principles enabling these tradeoffs. We believe the design in [?] is very aggressive and may not be feasible considering the state-of-the-art in device technology. On the other hand, if the micro second level retention time is feasible, then our proposed architectural solution would be even more beneficial.

An application-driven study to determine retention time: We analyze the time between writes or replacements to a cache line for various multi-threaded and multi-programmed workloads. Our characterization augments the prior body of work that analyzes cache lifetimes mainly in single processor and single program configurations. Based on the L2 cache behavior, we propose to design STT-RAMs with retention time in the range of 10ms.

Architectural solution to handle STT-RAM volatility: We present a simple buffering mechanism to ensure the integrity of programs given the volatile nature of our tuned STT-RAM cells. Experimental results with PARSEC and SPEC benchmarks on a four-core and eight-core multicore platform compared to a base case 1MB SRAM per core and the ideal 4MB SRAM per core indicate that the proposed solution is attractive both from performance and power perspectives. (Summarize the results here)

The rest of this paper is as follows:

2. STT-RAM Design

2.1. Preliminary on STT-RAM

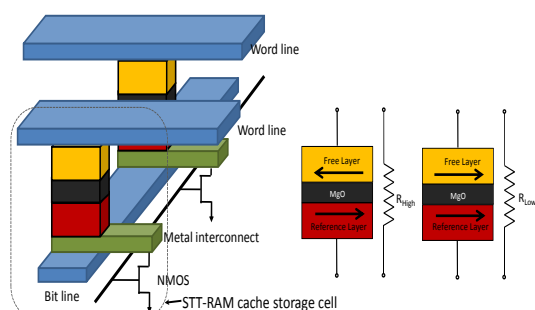


Figure 1. (a) Structural view of STT-RAM Cache Cell (b) Anti Space Parallel (High Resistance, Indicating "1" state) (c) Parallel (Low Resistance, Indicating "0" state)

STT-RAM uses Magnetic Tunnel Junction (MTJ) as the memory storage and leverages the difference in magnetic directions to represent the memory bit. As shown in Fig. 1, MTJ contains two ferromagnetic layers. One ferromagnetic layer has fixed magnetization direction and it is called the reference layer, while the other layer has a free magnetization direction that can be changed by passing a write current and it is called the free layer. The relative magnetization direction of two ferromagnetic layers determines the resistance of MTJ. If two ferromagnetic layers have the same directions, the resistance of MTJ is low, indicating a "1" state; if two layers have different directions, the resistance of MTJ is high, indicating a "0" state.

As shown in Fig. 1, when writing "0" state into STT-RAM cells, positive voltage difference is established between SL and BL; when writing "1" state, vice versa. The current amplitude required to reverse the direction of the free ferromagnetic layer is determined by the size and aspect ratio of MTJ and the write pulse duration.

2.2. Write current versus write pulse width trade-off

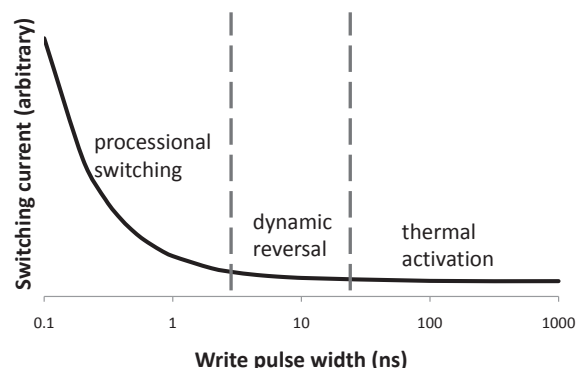


Figure 2. (a) Structural view of STT-RAM Cache Cell (b) Anti Space Parallel (High Resistance, Indicating "1" state) (c) Parallel (Low Resistance, Indicating "0" state)

STT-RAM uses Magnetic Tunnel Junction (MTJ) as the memory storage and leverages the difference in magnetic directions to represent the memory bit. As shown in Fig. 1, MTJ contains two ferromagnetic layers. One ferromagnetic layer has fixed magnetization direction and it is called the reference layer, while the other layer has a free magnetization

direction that can be changed by passing a write current and it is called the free layer. The relative magnetization direction of two ferromagnetic layers determines the resistance of MTJ. If two ferromagnetic layers have the same directions, the resistance of MTJ is low, indicating a "1" state; if two layers have different directions, the resistance of MTJ is high, indicating a "0" state.

As shown in Fig. 1, when writing "0" state into STT-RAM cells, positive voltage difference is established between SL and BL; when writing "1" state, vice versa. The current amplitude required to reverse the direction of the free ferromagnetic layer is determined by the size and aspect ratio of MTJ and the write pulse duration.

The current amplitude required to reverse the direction of the free ferromagnetic layer is determined by a lot of factors such as material property, device geometry and importantly the write pulse duration. Generally, the longer the write pulse is applied, the less the switching current is needed to switch the MTJ state. Three distinct switching modes were identified [3] according to the operating range of

switching pulse width τ : thermal activation ($\tau > 20ns$), precessional switching ($\tau < 3ns$) and dynamic reversal ($3ns < \tau < 20ns$).

The relationship between switching current density J_c and write pulse width τ was characterized by an analytical model in [10]. The equations are listed as follows,

$$J_{c,TA}(\tau) = J_{c0} \left\{ 1 - \left(\frac{k_B T}{E_b} \right) \ln \left(\frac{\tau}{\tau_0} \right) \right\} \quad (1)$$

$$J_{c,PS}(\tau) = J_{c0} + \frac{C}{\tau^\gamma} \quad (2)$$

$$J_{c,DR}(\tau) = \frac{J_{c,TA}(\tau) + J_{c,PS}(\tau) e^{-k(\tau - \tau_c)}}{1 + e^{-k(\tau - \tau_c)}} \quad (3)$$

where $J_{c,TA}$, $J_{c,PS}$, $J_{c,DR}$ are the switching current densities for thermal activation, precessional switching and dynamic reversal respectively. J_{c0} is the critical switching current density, k_B is the Boltzmann constant, T is the temperature, E_b is the thermal barrier, and τ_0 is inverse of the attempt frequency. C , γ , k , and τ_c are fitting constants. Based on the observation from Fig. 2 and analysis of the analytical model, we found very different switching characteristics in the three switching modes. For example, in thermal activation mode, the required switching current increases very slowly even we decrease the write pulse width by orders of magnitude, thus short write pulse width is more favorable in this regime because reducing write pulse can reduce both write latency and energy without much penalty on read latency and energy. While in precessional switching, write current goes up rapidly if we further reduce write pulse width, therefore minimum write energy of the MTJ is achieved at some particular write pulse width in this regime. Consequently, this paper will focus on the exploration of write pulse width in precessional switching and dynamic reversal to optimize for different design goals.

2.3. STT-RAM Modeling

To simulate the performance of STT-RAM cache, it is important to estimate its cell area first. As mentioned before, each 1T1J STT-RAM cell is composed of one NMOS and one MTJ. The NMOS access device is connected in series with the MTJ. The size of NMOS is constrained by both SET and RESET current, which are inversely proportional to the writing pulse width. In order to estimate the

current driving ability of MOSFET devices, a small test circuit using HSPICE with PTM 45nm HP model [13] is simulated. The BL-to-SL current and SL-to-BL current are obtained by assuming typical TMR (120%) and LRS ($3k\Omega$) value [9] and bursting wordline voltage to be 1.5V (the optimal value is extracted from [2]). And we over size the access transistor width to guarantee enough write current provided to MTJ using the methodology discussed in [12]. To achieve high cell density, we model the STT-RAM cell area by referring to DRAM design rules [7]. As a result, the cell size of a STT-RAM cell is calculated as follows,

$$\text{Area}_{\text{cell}} = 3(W/L + 1)(F^2) \quad (4)$$

2.4. Impact of MTJ Retention Time on STT-RAM

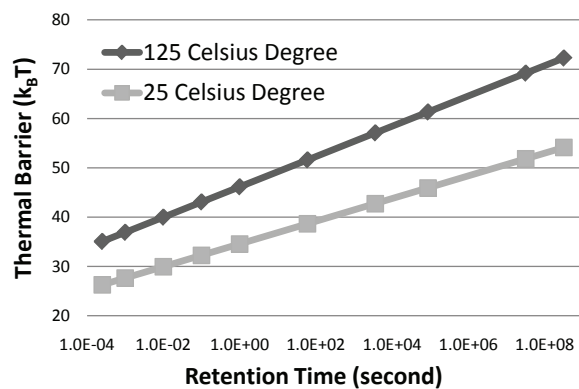


Figure 3. MTJ thermal stability requirement for different retention time

cell but also on the write current. It was found in [8] that the switching current of MTJ increases almost linearly with thermal barrier when thermal barrier is $< 70k_B T$, where k_B is the Boltzman constant and T is temperature. Here we combine this observation with the write current versus write time trade-off described in Section 2.2, which essentially means that once the thermal barrier of a MTJ is lowered we are able to achieve faster write speed or/and smaller write current/energy. The most straightforward way to reduce thermal barrier is to tune device geometry such as planar area, thickness of free layer and aspect ratio of the elliptic MTJ.

The retention time of a MTJ is largely determined by the thermal stability of the MTJ. The relation between retention time and thermal barrier is captured in Figure 3, which can be modeled as $t = C \times e^{k\Delta}$, where t is the retention time and Δ is the thermal barrier while C and k are fitting constants. Thermal stability of the free layer in an MTJ does not only have impact on retention time of STT-RAM memory

Table 1. 16-way L2 Cache Simulation Results

			Area (mm^2)	Read Latency (ns)	Write Latency (ns)	Read Energy (nJ)	Write Energy (nJ)	Leakage Power (mW)
1MB SRAM			2.612	1.012	1.012	0.578	0.578	4542
4MB STT-RAM	$t = 10yr$	Leakage Opt.	2.628	2.434	4.919	0.635	0.663	1399
		Latency Opt.	3.003	0.998	10.61	1.035	1.066	2524
	$t = 1s$	Leakage Opt.	2.203	2.044	3.552	0.589	0.616	1388
		Latency Opt.	2.904	0.973	5.571	1.015	1.036	2235
	$t = 100ms$	Leakage Opt.	2.181	1.994	3.432	0.575	0.608	1250
		Latency Opt.	2.902	0.963	3.002	1.008	1.021	2230
	$t = 10ms$	Leakage Opt.	2.167	1.956	3.390	0.571	0.601	1151
		Latency Opt.	2.901	0.959	2.598	1.002	1.028	2227

2.5. STT-RAM Cache Simulation Setup

We simulate SRAM-based caches and STT-RAM-based caches with a tool called NVsim [4], which is a circuit-level performance, energy, and area simulator based on CACTI for emerging non-volatile memories. All the models described in this Section has been integrated in NVsim. The simulation results are listed in Table 1. We can see that the leakage-optimized 4MB non-volatile STT-RAM cache has almost the same area with 1MB SRAM. This is consistent with previous work [5]. By relaxing retention time of STT-RAM with lower thermal barrier, the leakage-optimized STT-RAM cache can have smaller area, faster write latency and less leaky peripheral circuitry. However, as retention time is exponentially related with thermal barrier and thermal barrier is extremely sensitive to process variation and temperature, the benefit of decreasing write latency by relaxing the retention time in the same order (i.e. from 50ms to 10ms) is so small which may be offset by slight variation in device geometry or environment temperature. Moreover, the intrinsic fluctuations in CACTI make it very difficult to observe that small benefit as well. Another point worth mentioning is that the read latency of leakage-optimized 4MB STT-RAM cache is significantly larger than 1MB SRAM cache because sensing the state of STT-RAM cell takes longer and fast SRAM sensing. Thus, we reduce the array size to improve the latency of STT-RAM cache. As can be seen in Table 1, the latency-optimized STT-RAM cache has noticeable better read and write latency with 14% – 34% area overhead about 40% dynamic energy overhead compared to leakage-optimized STT-RAM cache with the same retention time.

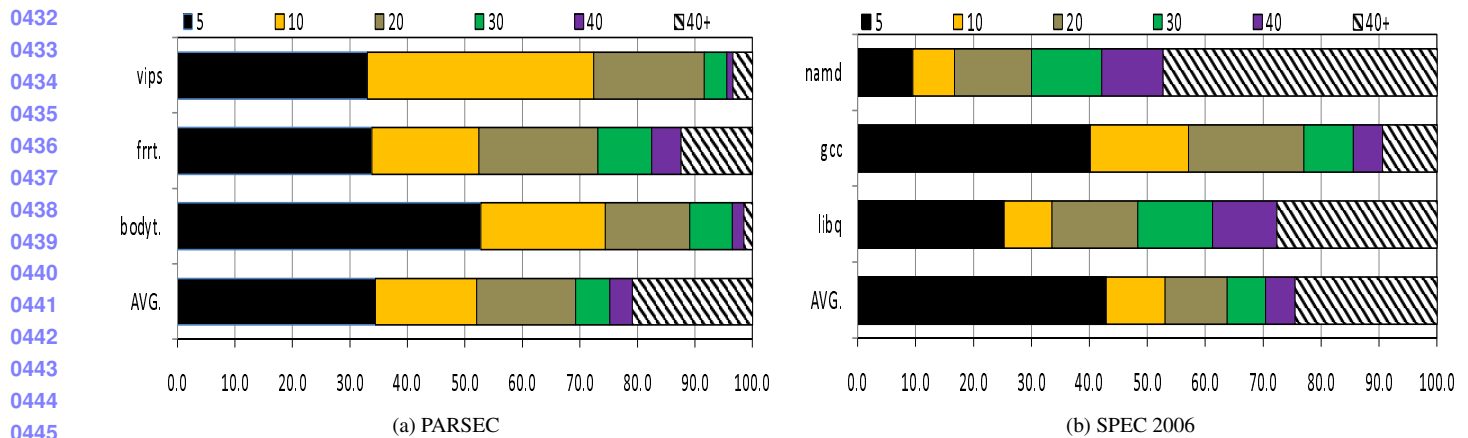


Figure 4. Distribution of Blocks Showing Different Revival Times

3. Understanding tradeoffs of Retention Time

In order to utilize the volatile STT-RAM as the last level cache in designing an effective cache hierarchy, we need to know what should be the ideal/feasible retention time. Ideally, the STT-RAM write latency should be competitive to SRAM latency and the cache retention time should be high. However, as discussed in the following section, since the write latency is inversely proportional to the retention time, we need to find a feasible tradeoff based on the STT-RAM device characteristics. Thus, we first attempt to decide an ideal retention time by analyzing the characteristics of a last level cache in a multi-programmed environment. The idea is to understand the distribution of the inter-write interval and thus the average inter-write time to a last level cache and use this time as the STT-RAM retention time. This section describes our application-driven study to estimate the retention time.

3.1. Relating Application Characteristics to Retention Time

Application characterization gives the basis for evaluating the impact of retention time on the overall system performance. In order to do this characterization, the first step is to find an ideal time for which the cache block should retain the data. A cache block is only refreshed when the block is written. Thus, we record intervals between two successive writes (refreshes) to the same L2 cache block. We define this interval to be *revival time*. While collecting these results, we ensure that if a block gets invalidated in between two consecutive writes, we don't consider the time in between the invalidation and the next write. Previous works [?] do similar type of revival time analysis, but for L1 cache. Figure 4 shows

Table 2. Retention and Write Latencies for STT-RAM L2 Cache

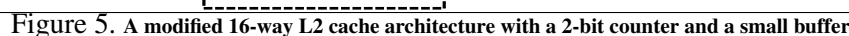
Retention Time	10years	1sec	10ms
Write Latency (Latency Optimized) @2GHz	22 cycles	12 cycles	6 cycles
Write Latency (Leakage Optimized)@2GHz	10 cycles	8 cycles	8 cycles

the distribution of L2 cache blocks having different revival time intervals. These results are obtained by running multi-threaded (PARSEC [?]) and multi-programmed (SPEC 2006 [?]) applications on the M5 Simulator [?] that models a 2GHz processor consisting of 4 cores, with 4MB L2 cache. Table 3 contains additional details of the system configuration. Figures 4 (a) and (b) show the results of three PARSEC and SPEC benchmarks along with the averages across 12 PARSEC and 14 SPEC benchmarks, respectively. We observe from the figure that, on an average, approximately 50% of cache blocks get refreshed within 10 ms, this is in contrast to the microsecond reuse for L1 case [?]. About 20% of blocks remain in the cache for more than 40 ms and rest of the blocks have intermediate revival times. We conclude that blocks which stay longer than the retention time in the cache without being refreshed are assumed to be not available, and would affect the application performance the most. This distribution also gives us the basis on which we can choose the optimal retention time. Reducing the retention time too much will make the cache too volatile leading to degraded performance, while increasing the retention time would affect the write latency. In the next subsection, we will see how increasing the retention time, has negative impacts on write latency.

3.2. Low Retention STT-RAM Characteristics

Table 2 shows that there is significant reduction in write latency with reduction in retention time. Section 4 explains how these numbers originate. We want to clarify from device fabrication perspective that, these retention times are the most stable designs possible. As we lower the retention times of these STT-RAM cells in the range of *ms* it becomes much harder to precisely mark a STT-RAM cell with a fixed retention time. For the sake of correctness and preciseness we discuss these designs only in the paper. Later in the Section 7, it will be clear, that our design assumptions have no affect on the generality of the results.

To analyze the tradeoffs between retention time and overall system performance, lets consider an



4. Architecting Volatile STT-RAM

11

blocks to more sophisticated schemes, where we minimize the number of refreshes and write backs.

4.1. Volatile STT-RAM

In this naive design, we write back all the dirty blocks which are going to expire. To identify these blocks, we maintain a counter per cache block. To understand the working of the counter, let us consider a n bit counter. We assume the time between transitions (T) from one state to another equals to the retention time divided by the number of states, where the number of states is 2^n . The block is put in S_0 state when it is first written. After every transition time (T), the counter of each block is incremented. When the block reaches S_{n-1} , it indicates that it is going to expire in time T . We define this time as *alert time* and the block in state S_{n-1} as diminishing block. Increasing the value of n , will decrease the alert time at the cost of increased overhead of checking blocks at finer granularity.

Our experimental results show that a 2 bit counter similar to the one used in [?] is sufficient enough to detect the expiration time of the block. The block can be in one of the four states as shown in the figure 5 (b). Counter bits are kept as a part of the SRAM tag array. We calculate the overhead of 2 bit counters to be 0.4% over one L2 cache bank. Volatile STT-RAM scheme has negative impact on the performance for two reasons: (1) There will be large number of write backs to the main memory. (2) The expired block could have been frequently read and losing it will incur additional read misses. We evaluate the results of this design in Section 7.

4.2. Revived STT-RAM Scheme

Figure 5 a) shows the schematic diagram of the overall architecture design of this scheme. The main components of this design are:

Buffer: It is a per bank small storage space with fixed number of entries made up of low-retention time STT-RAM cells. We use these entries to temporarily store the diminished blocks. We estimate the optimal buffer size later in the section.

Buffer Controller: Buffer controller consists of a buffer overflow detector of $\log_2 N$ bits where N is the buffer size. If a diminishing block is directed to the buffer, the overflow detector is first checked to see the occupancy of the buffer. If the buffer is not full, the block is copied to one of the empty buffer entries

Table 3. **Baseline processor, cache, memory and configuration**

Processor Pipeline	2 GHz processor, 64-entry instruction window, Fetch/Exec/Commit width 8
L1 Caches	64 KB per-core (private), 4-way set associative, 64B block size, write-back, split I/D caches, 10 MSHRs
L2 Caches	1MB banks, shared, 16-way set associative, 64B block size, 4-cycle bank latency, 10 MSHRs
Main Memory	4GB DRAM, up to 16 outstanding requests for each processor, 400 cycle access

along with set and way id. If the buffer is full, the dirty blocks are written back to the main memory, otherwise it is invalidated. The buffer overflow detector is also incremented by one.

Implementation Details: Figure 5 (a) shows 16-way set associative cache bank with associated tag array. Counter bits are also placed in tag array. We show the working of our scheme using a 2 bit counter. One of the sets, is shown in detail to clarify the details of the scheme. All the blocks in the way are marked with their current state. Each bank is associated with a buffer and buffer controller. Let us consider that we are using buffering scheme for eight MRU slots. Later in this section, we will justify this decision. In Section 7, we will vary the number of slots to see the effects on the performance.

Illustration of the scheme: ❶ shows that three blocks in first eight MRU slots are diminishing and directed to the buffer. ❷ checks the occupancy of the buffer and if it is not full, they are copied to one of the entries of ❸ along with way and set id. Way and set id are again used by the ❷ to copy back the blocks to the same place from where they brought from. ❹ shows the blocks which are not in MRU slots, but are diminishing. We check these blocks in ❺ to see whether they are dirty or not. If they are dirty we first write back those blocks as shown in ❻. If they are not dirty, it is invalidated.

Choosing Optimal Buffer and MRU Slots: In order to calculate the optimal MRU slots for buffering, we collected statistics of MRU positions of diminishing blocks by running various PARSEC and SPEC Benchmarks on the M5 Simulator. Figure 6 shows the average cumulative distribution of expired blocks per bank varying with number of ways in a set. We observe that, number of diminished blocks become stable after first eight MRU ways. The mean number of blocks corresponding to the first eight ways is 2048 (3.16% overhead over per L2 cache bank), which is a good initial choice as the size of buffer. In sensitivity analysis we will fine tune the buffer size to minimize buffer overflows.

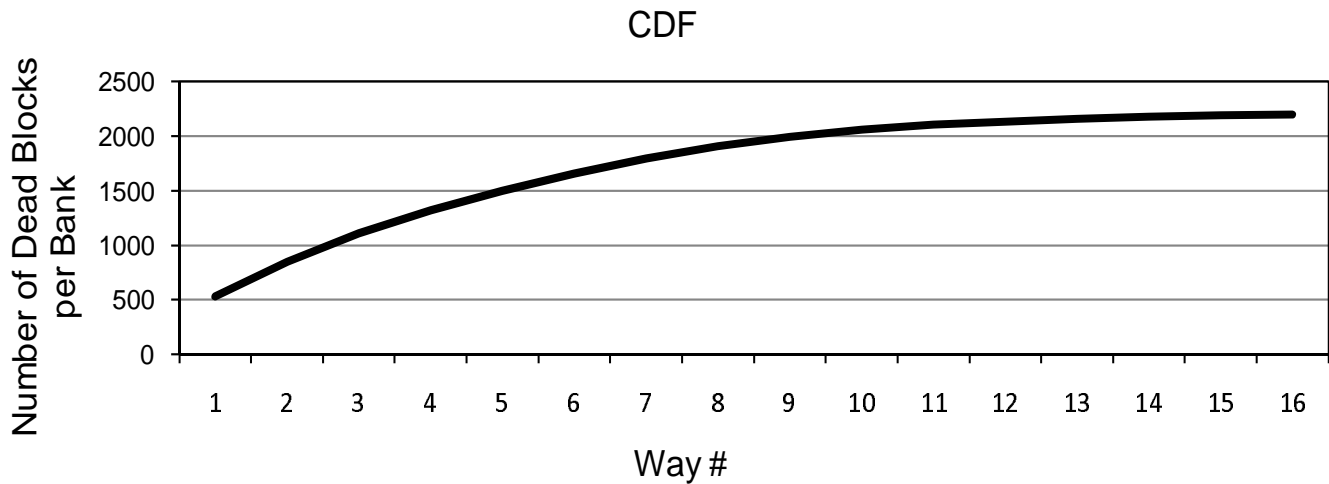


Figure 6. CDF

5. Experimental Evaluation

Experimental Setup We evaluate our design and schemes on the modified ALPHA M5 Simulator [1]. We operate M5 Simulator in Full System (FS) mode for PARSEC applications and in System Emulation (SE) Mode for SPEC 2006 Multiprogrammed mixes. We model a 2GHz processor with four out of order cores. We modified M5 simulator to model low retention time STT-RAM for L2 cache. The L2 cache is banked with different read and write latencies, with all the banks connected via a shared memory bus. We assume a fixed 400 cycles main memory latency for all our simulations. Table 3 details our experimental system configuration.

Collection of Results We report results of 12 multithreaded PARSEC applications and 14 SPEC 2006 multiprogrammed mixes. Table ?? shows the characterization of PARSEC applications and list of multiprogrammed mixes. We use sim-small input for PARSEC benchmarks and report the results of only Region of Interest (ROI) after skipping the initialization and termination phases (except facesim, where we report results for only 2B instructions of ROI) We also warm up caches for 100M Instructions in ROI. For SPEC multiprogrammed mixes, we fast forward 1B Instructions, warm up caches for 500M instructions and then report results for 1B instructions.

Performance Metrics For multithreaded PARSEC applications, we assume 4 threads are mapped to our modeled processor with four cores. We report normalized speedup for these applications, which is defined as the decrease in execution time of the slowest thread. We randomly choose 14 multiprogram

mixes, each mix with four different applications and assign each every application to a core. We report Instruction throughput and Weighted Speedup for SPEC multiprogrammed mixes, which are defined as:

6. Results

7. Prior Work

[ADWAIT, MORE STT-RAM RELATED WORK other than HPCA 2011 paper ESPECIALLY FOR STT-RAM CACHE DESIGN should be put here]

Moreover, in [11] the authors relax retention time of STT-RAM from 10years to $56\mu\text{s}$ by reducing the planar area of MTJ from $32F^2$ to $10F^2$. However, the scope of this work is limited by addressing practical device parameters and their variabilities. First, the retention time of MTJ is exponentially proportional to the thermal barrier, which makes the retention time of individual STT-RAM device extremely sensitive to any factor that has impact on thermal barrier, particularly device geometry. Thus it's important to take practical values of device geometry such as MTJ planar area and take their process variations into consideration. We get these parameters and corresponding variabilities from fabricated STT-RAM published in recent years [8, 1, 9, 6]. These state-of-the-art MTJs has much smaller baseline planar area that is around $2F^2$. Therefore there is not too much room to reduce retention time by aggressively reduce MTJ planar area. In this paper, we focus on the MTJ with worst-case retention time larger than millisecond and optimize STT-RAM cache correspondingly. Our analysis in this paper reveals the granularities at which a device designer can reliably tune the data retention times.

8. Conclusions

9. Conclusion

Spin-Transfer Torque RAM (STT-RAM) is a promising candidate for future on-chip cache design due to its high-density, low leakage, and immunity to soft errors. However, it's high write latency and dynamic write energy are the disadvantages compared to SRAM-based cache design. In this paper, we propose to trade off the non-volatility (data retention time) for better write performance/energy in

STT-RAM cache design. We study two data-retention relaxation cases, one with data retention time of 1 second, which satisfies the lifetime requirement of typical cache blocks; and the other one with data retention time of 1ms, which is a more aggressive design for better performance/energy gains but a data refreshing mechanism is needed. Our experimental results show that.....

References

- [1] P. Amiri, Z. Zeng, P. Upadhyaya, G. Rowlands, H. Zhao, I. Krivorotov, J.-P. Wang, H. Jiang, J. Katine, J. Langer, K. Galatsis, and K. Wang. Low write-energy magnetic tunnel junctions for high-speed spin-transfer-torque MRAM. *IEEE Electron Device Letters*, 32(1):57–59, 2011. 15
- [2] S. Chatterjee, M. Rasquinha, S. Yalamanchili, and S. Mukhopadhyay. A scalable design methodology for energy minimization of STT-RAM: a circuit and architecture perspective. *IEEE Transactions on Very Large Scale Integration*, 2010. 7
- [3] Z. Diao, Z. Li, S. Wang, Y. Ding, A. Panchula, E. Chen, L.-C. Wang, and Y. Huai. Spin-transfer torque switching in magnetic tunnel junctions and spin-transfer torque random access memory. *Journal of Physics: Condensed Matter*, 19(16):165209, 2007. 5
- [4] X. Dong, N. P. Jouppi, and Y. Xie. PCRAMsim: System-level performance, energy, and area modeling for phase-change RAM. In *Proceedings of the International Conference on Computer-Aided Design*, pages 269–275, 2009. 8
- [5] X. Dong, X. Wu, G. Sun, Y. Xie, H. Li, et al. Circuit and Microarchitecture Evaluation of 3D Stacking Magnetic RAM (MRAM) as a Universal Memory Replacement. In *Proceedings of the Design Automation Conference*, pages 554–559, 2008. 8
- [6] A. Driskill-Smith. Latest Advances in STT-RAM. In *2nd Annual Non-Volatile Memories Workshop*, 2011. 15
- [7] F. Fishburn, B. Busch, J. Dale, D. Hwang, et al. A 78nm 6F² DRAM technology for multigigabit densities. In *Proceedings of the Symposium on VLSI Technology*, pages 28–29, 2004. 7
- [8] T. Kishi, H. Yoda, T. Kai, T. Nagase, E. Kitagawa, M. Yoshikawa, K. Nishiyama, T. Daibou, M. Nagamine, M. Amano, S. Takahashi, M. Nakayama, N. Shimomura, H. Aikawa, S. Ikegawa, S. Yuasa, K. Yakushiji,

- H. Kubota, A. Fukushima, M. Oogane, T. Miyazaki, and K. Ando. Lower-current and fast switching of a perpendicular TMR for high speed and high density spin-transfer-torque MRAM. In *Proceedings of International Electron Devices Meeting*, pages 1–4, 2008. 7, 15
- [9] C. Lin, S. Kang, Y. Wang, K. Lee, X. Zhu, W. Chen, X. Li, W. Hsu, Y. Kao, M. Liu, Y. Lin, M. Nowak, N. Yu, and L. Tran. 45nm low power CMOS logic compatible embedded STT MRAM utilizing a reverse-connection 1T/1MTJ cell. In *Proceedings of International Electron Devices Meeting*, pages 57–59, 2009. 7, 15
- [10] A. Raychowdhury, D. Somasekhar, T. Karnik, and V. De. Design space and scalability exploration of 1T-1STT MTJ memory arrays in the presence of variability and disturbances. In *Proceedings of International Electron Devices Meeting*, pages 707–710, 2009. 6
- [11] C. W. Smullen, V. Mohan, A. Nigam, S. Gurumurthi, and M. R. Stan. Relaxing non-volatility for fast and energy-efficient STT-RAM caches. In *Proceedings of the International Symposium on High Performance Computer Architecture*, pages 50–61, 2011. 15
- [12] W. Xu, H. Sun, X. Wang, Y. Chen, and T. Zhang. Design of last-level on-chip cache using spin-torque transfer RAM (STT RAM). *IEEE Transactions on Very Large Scale Integration*, 19(3):483–493, 2011. 7
- [13] W. Zhao and Y. Cao. New generation of predictive technology model for sub-45 nm early design exploration. *IEEE Transactions on Electron Devices*, 53(11):2816–2823, nov. 2006. 7